ORIGINAL RESEARCH ARTICLE

Does a Low Amount of Substituents Improve the Thermoelectric Properties of Cr$_{2-x}$M$_x$S$_3$ (M = Ti, V, Sn)?

Hendrik Groß[1] · Yeliz Ekici[1] · Michael Poschmann[2,3] · Dennis Groeneveld[4] · Torben Dankwort[1,5] · Jan D. Koenig[4,6] · Wolfgang Bensch[2] · Lorenz Kienle[1]

Abstract

The effects of low-level partial cation substitution in Cr$_{2-x}$M$_x$S$_3$ with M = Ti, V or Sn and $x = 0.05$ and 0.1 have been investigated regarding the long- and short-range crystal structures and thermoelectric properties. All substituted compounds crystallized in the equilibrium phase of Cr$_2$S$_3$, adopting the space group $R\bar{3}$. Electron beam irradiation led to a phase transformation from space group $R\bar{3}$ to $P\bar{3}1c$ with a subsequent appearance of diffuse scattering, indicating short-range ordering of cations in the partially occupied cation layers. Substitution of Cr by V led to a reduction in electrical conductivity and subsequently to a lower thermoelectric performance in comparison to the pristine material. In contrast, substitution with Ti yielded an improvement of the performance due to a higher electrical conductivity and a reasonably high Seebeck coefficient. Both Sn-substituted compounds contained only traces of Sn. Surprisingly, a significant improvement of the electrical conductivities could be observed in comparison to the pristine material as well as the other Cr$_{2-x}$M$_x$S$_3$ materials.

Introduction

Following the global trend of finding new sources of energy, thermoelectric materials have lately gained interest as a possible means of renewable, continuous energy generation from waste heat. Established materials such as Bi-, Sb-, and Pb-based tellurides generally show promising efficiencies. However, these materials are not environmentally friendly, and specifically, Te is not an abundant on earth, making large-scale applications unlikely.[1–7] Hence, current research in thermoelectrics focuses on identifying alternative materials with similar efficiencies, while providing a lower environmental impact and consisting of earth-abundant elements.[1] One class of materials that cover these criteria are small band gap chromium sulfides with $E_{gap} \sim 37(6)$ meV for Cr$_2$S$_3$ and $E_{gap} \sim 44(1)$ meV for a sulfur-deficient phase.[8,9] Although indeed exhibiting a lower efficiency than established materials, these compounds show a plethora of possibilities for improvements due to their structural and chemical variability.[10–19] This in turn may enable tuning of the Seebeck coefficient, electrical and thermal conductivities. One of these possibilities, and also the main subject of this study, is the low-level substitution of the Cr^{3+} cations by other elements. The substitution alters the properties of the material in a way that the electrical conductivity is specifically affected. In general, the structures of chromium sulfides Cr$_{1-x}$S are derivatives of the NiAs-type structure (space group $P6_3/mmc$), in which Cr atoms are removed in an ordered way from every second cation layer parallel to the crystallographic c-axis. As a result, the structure comprises layers of edge-sharing CrS$_6$ octahedra, alternating with layers that are only partially occupied by cations.[8] These

✉ Lorenz Kienle
  lk@tf.uni-kiel.de

[1] Institute for Materials Science, Kiel University, Kaiserstr. 2, 24143 Kiel, Germany

[2] Institute for Inorganic Chemistry, Kiel University, Max-Eyth-Str. 2, 24118 Kiel, Germany

[3] Max Planck Institute for Chemical Energy Conversion, Stiftstraße 34-36, 45470 Mülheim an der Ruhr, Germany

[4] IMTEK – Department of Microsystems Engineering, University of Freiburg, Georges-Koehler-Allee 102, 79910 Freiburg, Germany

[5] Fraunhofer Institute for Silicon Technology ISIT, Fraunhoferstraße 1, 25524 Itzehoe, Germany

[6] Fraunhofer Institute for Physical Measurement Techniques IPM, Georges-Koehler-Allee 301, 79110 Freiburg, Germany

structural features facilitate a low lattice thermal conductivity orthogonal to the lattice planes,[20,21] while the cation arrangement in the partially occupied layers is well suited for doping and chemical substitution without transforming the initial crystal structure.[22–24] Cr_2S_3, which serves as the base material for the presented study, crystallizes in two different polymorphs, whose respective structures are depicted in Fig. 1.

The rhombohedral modification of Cr_2S_3, which crystallizes in space group $R\bar{3}$, is the thermodynamic equilibrium phase.[25] The primitive trigonal phase, crystallizing in space group $P\bar{3}1c$, often appears after compacting the material via field-assisted sintering (FAST). This results from an undesired volatilization of sulfur during the procedure, leading to sulfur-deficient Cr_2S_{3-x}.[26,27] In order to maintain the rhombohedral phase while still achieving a good densification necessary for high electrical transport properties,[28,29] parameters developed in a previous study[30] have been applied in the sintering process.

The key strategy to tailor and improve the thermoelectric properties of materials is achieving the highest-possible electrical conductivity and Seebeck coefficient while keeping the thermal conductivity as low as possible.[7] As Cr_2S_3 generally exhibits semiconducting behavior,[26,27] enhancements in both directions can be made. Since the thermal conductivity is directly linked to phonon propagation in the crystal lattice, it can be effectively reduced via the introduction of phonon-scattering objects such as structurally incompatible atoms or precipitations.[31–34] The electrical conductivity, on the other hand, may be enhanced by doping the material with elements of a different number of electrons for electron delocalization.[10] In this particular study, Ti^{3+} and V^{3+} have been selected as substituents for Cr^{3+} due to their lower number of d-electrons in the oxidation state +3, while they are structurally compatible due to their smaller ionic radii. Sn^{2+}/Sn^{4+} has been chosen specifically as a structurally incompatible element and is expected to generate nanoscale precipitations.

Vanadium sulfides cover a similar range of chemical composition as Cr sulfides and crystallize in NiAs-type-related structures. In contrast to Cr sulfides, however, the V sulfides show metallic properties.[35,36] It was demonstrated that the electrical properties of Cr sulfides can be significantly altered if Cr is substituted by V. For $V_xCr_{2-x}S_3$, the rhombohedral structure of Cr_2S_3 is maintained for $0 < x \leq 0.75$, while for larger x values > 1.6, a single-phase region with a cation-deficient Cr_3S_4-like structure is observed.[10] For all other members of the series, a two-phase region was found. The electrical properties of the $V_xCr_{2-x}S_3$ phases with $0 < x \leq 0.75$ indicate semiconducting behavior, while compounds with $x > 1.6$ show metallic behavior.[10] The electric transport in $V_xCr_{2-x}S_3$ phases with $0 < x \leq 0.75$ is characterized by a variable range hopping mechanism.[37]

The compound Ti_2S_3 was reported to crystallize in a NiAs-type defect structure as well, being comprised of Ti-deficient layers that alternate with fully occupied layers.[38,39] Several superstructures were also reported for Ti_2S_3.[40] Not much is known about the physical properties of this compound, but it is accepted that Ti occurs as Ti^{3+} (d^1).
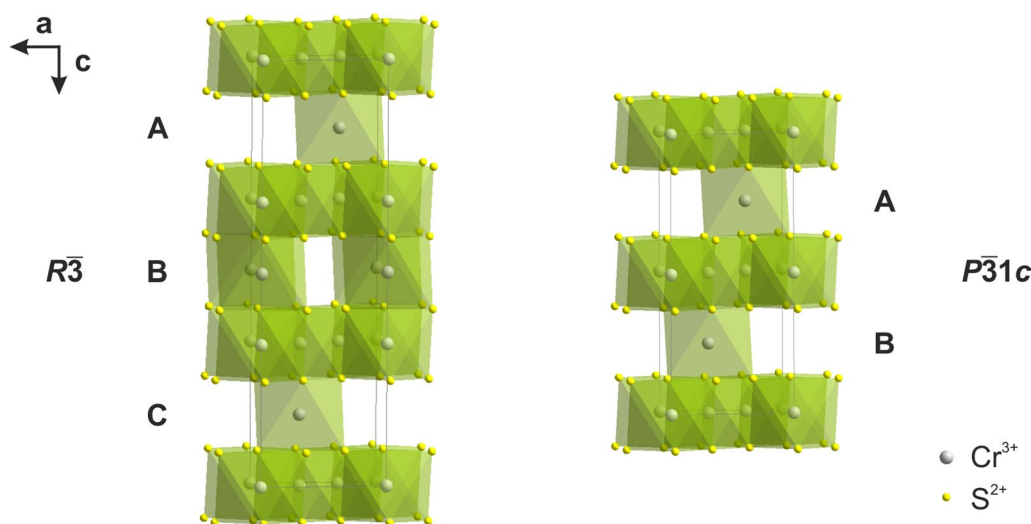
Fig. 1 Structural representation of Cr_2S_3 in the rhombohedral $R\bar{3}$ (left) and trigonal $P\bar{3}1c$ (right) phases, viewed along b-direction. Letters A, B and C indicate partially occupied and differently stacked layers of Cr atoms. While both phases share the basic setup of fully occupied layers of CrS_6 octahedra, they differ in the sequence of partially occupied cation layers. The $R\bar{3}$ structure follows an A-B-C sequence of the cation layers, which is reduced to an A-B stacking in $P\bar{3}1c$. The resulting unit cell shares the same metrics except for the c-axis. Structure models are based on reference data from Ref. 25,26.

The tin monosulfide SnS exhibits polymorphism with an orthorhombic[41] and a cubic variant.[42] Recently, a cubic polymorph with a superstructure was reported, containing 64 atoms within the unit cell.[43] All these variants are semi-conducting and contain Sn in the oxidation state +2. The sesquisulfide Sn_2S_3 is a mixed-valency compound featuring Sn^{2+} and Sn^{4+}.[44]

Based on this analysis, one can assume that Cr^{3+} can be substituted by V^{3+} and Ti^{3+}, but not by Sn^{2+} or Sn^{4+}, and one may expect that Sn sulfide is segregating. In order to elaborate the influence of substitutions of the Cr cations in Cr_2S_3, we restricted the compositional range to either 5% or 2.5% of the pristine Cr content. The samples were synthesized by a high-temperature solid-state reaction, and the products were compacted via FAST. The resulting materials were electrically characterized and investigated with respect to alterations of the crystal structures and the thermoelectric properties.

Experimental

Materials

Chromium (Alfa Aesar, 325 mesh, 99%), titanium (Sigma Aldrich, 100 mesh, 99.7%), sulfur (Alfa Aesar, > 99.9995%), tin (Alfa Aesar, 100 mesh, 99.999%) and vanadium (Chem-Pur, 200 mesh, > 99.5%) were stored under an argon atmosphere and used without further processing. All chemicals were used as purchased.

Synthesis and Sintering

The investigated samples were prepared in high-temperature synthesis. A stoichiometric mixture of pure elements was hand-ground and transferred into a quartz ampoule, which was subsequently evacuated (10^{-4} mbar). Heating was performed in a two-step process by heating the samples to 723 K with a rate of 45.2 K h^{-1}, holding there for 1 d and subsequently heating to 1273 K with a rate of 26.5 K h^{-1}. The temperature was held for 3 d, followed by cooling to room temperature. The obtained solid was ground and checked for purity using XRD.

The polycrystalline powders were compacted using a FAST device FCT Systeme HDP 5 at 1123 K and 395 MPa for 5 min with a heating and cooling rate of 100 K min^{-1} (pulsing) under an argon atmosphere. The high applied pressure and short holding time were chosen to prevent the volatilization of sulfur. With this method, it is possible to produce highly densified and phase-pure chromium sulfides, as could be demonstrated in a previous study.[30] The sintered samples had a diameter of 12.7 mm.

For x-ray diffraction (XRD) measurements, sintered samples were ground and thoroughly mixed in a 1:1 weight ratio with amorphous SiO_2 to reduce influences of x-ray absorption during XRD experiments. The mixtures were filled into 0.3 mm glass capillaries (Hilgenberg, wall thickness 0.01 mm) and the XRD patterns were measured with a PAN'alytical Empyrean MPD using Cu K_α irradiation, focusing mirror, fixed 1/4° divergence slit, fixed ½° anti-scatter slit and 2.292° Soller slit to adjust the incident beam. Diffracted beams were adjusted with a 2.292° Soller slit. X-ray diffraction patterns of sample pellets were measured with a PAN'alytical X'Pert MPD using Cu K_α irradiation. To adjust the incident beam, a Goebel mirror, fixed divergence slit 1/4°, fixed anti-scatter slit 1/2° and 2.292° Soller slit were used. A parallel plate collimator was used to remove diffuse x-rays from the scattered beam.

Rietveld refinements were done using the program Topas v6[45] in combination with the coding program jedit.[46] The profile function of the instrument was determined as a Thomson–Cox–Hastings pseudo-Voigt profile with additional simple axial model as implemented in Topas using a LaB_6 Standard Reference Material 660c (National Institute of Standards and Technology, NIST). Crystallographic data for Cr_2S_3 published by Jellinek[25] was used as initial values for refinements. Occurring Cr_2O_3 phases were refined with initial data published by Sawada.[47] Preferred orientation of crystallites was considered using the March-Dollase approach as supplemented by Zolotoyabko.[48–50]

Topography and surface composition of the samples were examined via scanning electron microscopy (SEM) in combination with energy-dispersive x-ray spectroscopy (EDX) and x-ray photoemission spectroscopy (XPS). The investigations were performed on a Zeiss Gemini Ultra 55 Plus equipped with an Oxford Instruments silicon drift (SD) detector. Samples for transmission electron microscopy (TEM) studies were taken from sintered pellets and thinned via mechanical grinding, dimpling and final polishing in a Gatan Precision Ion Polishing System (PIPS). TEM micrographs were obtained with a FEI Tecnai F30 G^2 with field emission gun (FEG) at 300 kV. Data evaluation was performed using Gatan Digital Micrograph 3.21 with additional scripts[51] as well as jems 4.7531 developed by Stadelmann.[52] Crystal structure visualizations were created with Diamond 3.2k by Crystal Impact.[53]

Density measurements were performed using an Archimedes setup at room temperature with ethanol as a suspending medium and the determined values were averaged over four measurements. The electrical conductivity and the Seebeck coefficient were measured perpendicular to the pressing direction with an uncertainty of 7% using the Netzsch SBA 458 Nemesis® under Ar atmosphere.[54] The thermal conductivity κ was determined according to $\kappa(T) = \rho(T) \cdot c_p(T) \cdot a(T)$, with the density ρ, the specific heat c_p and the

thermal diffusivity a with an uncertainty of 10%. The thermal diffusivity was measured via laser flash analysis (LFA), parallel to the pressing direction, with the Netzsch LFA 457 MicroFlash® under Ar atmosphere, and the specific heat was determined by using a reference specimen and is shown like the thermal diffusivity in Figure S7.

Sample Nomenclature

In the following, samples are labeled with an abbreviation representing their material and degree of substitution. Cr$_{1.9}$Sn$_{0.1}$S$_3$, e.g., corresponds to Sn01 and Cr$_{1.95}$Sn$_{0.05}$S$_3$ to Sn005, and the other substitutions with Ti and V are named accordingly.

Results

X-ray Diffraction

After the syntheses, the powdered samples consisted of $\geq$ 99 wt.% pure Cr$_2$S$_3$ and a negligible amount of Cr$_2$O$_3$ ($\leq$ 1 wt.%). In all samples, the structure of the samples adopted space group $R\bar{3}$ with small deviations of lattice parameters from literature values. When compared to data of similarly synthesized pure Cr$_2$S$_3$,[30] substitution of Cr by Ti or V caused a slight decrease in the lattice parameter a and a stronger increase in the c-axis, leading overall to an increased unit cell volume (see supporting information Table SI). The expansion of the unit cell can be explained by the larger ionic radii of Ti^{3+} and V^{3+} in comparison to Cr^{3+}, which is a typical effect observed for substituted Cr$_2$S$_3$.[10] Adding Sn did not change the lattice parameters by more than 0.04%, indicating absence of substitution. However, no additional tin sulfide or tin phase could be observed in XRD patterns, indicating the presence of amorphous phases or the removal of elemental tin during the high-temperature synthesis. The Rietveld refinements demonstrate that the metal atom position in the partially occupied metal atom layers exhibits a small deficiency (see supporting information Table SI). A partial occupation of the atomic position (2/3, 1/3, 0.5) instead of (0, 0, 0.5) is observed, resulting from disorder of interlayer Cr atoms or partial formation of Cr$_2$S$_3$ in $P\bar{3}1c$ (see supporting information Table SII). However, a small deficiency of interlayer Cr atoms is calculated, resulting in a mean ratio of Cr:S of 39.8:60.2. It must be noted that the occupation of the three metal atom sites by the different metal atoms could not be determined due to the low differences of the scattering power and the low content of the substituents.

After sintering, the preferred orientation of crystallites in sintered samples was determined by Rietveld refinements of XRD data collected in reflection geometry.[52] In all samples,

a preferred orientation of 12-38% of in-plane (00l)-layers was observed, and it is expected that this influences the conductivity characteristics of the samples. Higher preferred orientation was observed in Sn-containing samples, whereas a comparably low preferred orientation was observed for the V- and Ti-containing samples.

Because the physical properties would have been influenced by microstructural properties as well, small cuts of the pellets were ground and characterized via XRD and Rietveld refinements (see supporting information Figures S1-S5). As observed after the FAST process of oxidized samples under similar conditions,[55,56] all Cr$_2$O$_3$ impurities vanished, and all samples consisted of pure Cr$_2$S$_3$ phases (see Fig. 2).

According to the results of the Rietveld refinements, the samples obtained by the FAST process exhibited very similar trends for the unit cell volumes and lattice parameters as was observed for the as prepared samples. No pronounced differences in atomic positions were observed between as-prepared and FAST-treated samples (see supporting information Tables SII and SIII). Further, a deficiency in the occupancy of the chromium interlayer atomic position (0, 0, 0.5) was observed. The position is usually fully occupied in Cr$_2$S$_3$ in space group $R\bar{3}$. In all samples, the occupation of this position is reduced from 100 to ~ 83–91% (see Table I). Additionally, electron density was found on the atomic position (2/3, 1/3, 0.5). From this observation, occupational disorder and partial formation of Cr$_2$S$_3$ in space group $P\bar{3}1c$ can be reasoned. The change of the occupancies was possibly caused by the fast cooling at the end of the synthesis and
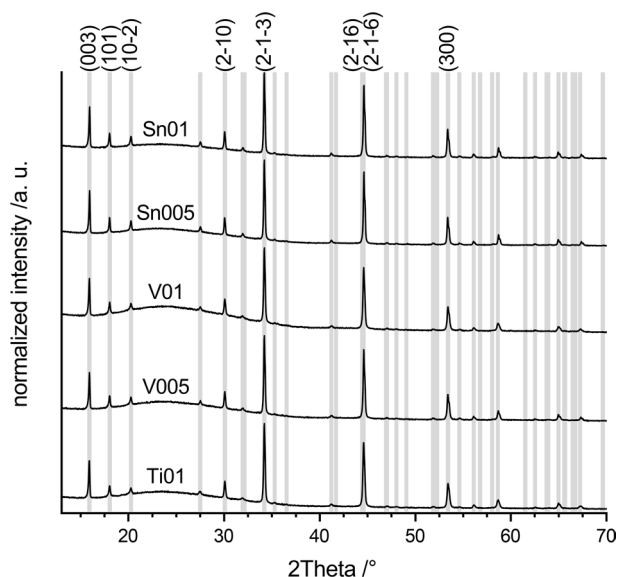
Fig. 2 XRD patterns measured of ground samples after FAST of Sn01-Ti01 top to bottom. Theoretical reflection positions of Cr$_2$S$_3$ in space group $R\bar{3}$, based on reference data from Ref. 25, are marked as grey lines. The most intense reflections are marked with corresponding Miller indices.

sintering procedure. This observation was more pronounced in samples containing V and Ti.

The observed isotropic microstrain was estimated as $\varepsilon_0 = 0.03$–0.06% and appeared to be influenced by substitution of Cr by Ti and V (see supporting information Table SIII).

All samples exhibited a relative density exceeding 95% (see supporting information Table SIV), calculated from the determined density of pellets divided by the theoretical density determined via Rietveld refinements.

Topography and Scanning Electron Microscopy

An investigation of pellet surfaces with SEM revealed that, with the exception of the V-containing materials V01 and V005, density and topography are comparable to pristine Cr_2S_3. As depicted in Fig. 3, the surfaces of samples Sn01

and Sn005 appeared to be nearly identical to the pristine material, samples V01 to Ti01 showed the incorporation of pores into the surface. These features were most evident for sample V01, where several coarse pores appeared, while sample V005 showed a finer dispersion. Sample Ti01 contained a minor number of visible pores, which, however, appeared far less frequently than in the V-substituted materials.

Further investigation of samples V01 and V005 found that they were brittle in comparison to the others and also contained visible cracks. The Cr-S stoichiometry, according to SEM-EDX, matched the desired 40-60 composition, while a small content of V and Ti could be detected throughout the respective samples. Interestingly, however, this was not the case for the Sn-containing samples 1 and 2, where no traces of the substituting element could be detected.

Table I Cell parameters determined from ground pellets via Rietveld refinement in comparison with literature data of similarly synthesized Cr_2S_3.[1]

	Cell parameters in Å		Volume in Å³	Preferential orientation η in %	Interlayer occupancy	
	a/b	c			(0; 0; 0.5)	(2/3; 1/3; 0.5)
Cr_2S_3[1]	5.9362 (6)	16.669 (3)	508.72 (1)	–		
$Cr_{1.9}Sn_{0.1}S_3$ (Sn01)	5.93831 (5)	16.6630 (2)	508.884 (12)	37.5 (11)	0.908 (3)	0.019 (2)
$Cr_{0.95}Sn_{0.05}S_3$ (Sn005)	5.93798 (5)	16.66260 (19)	508.805 (10)	28.3 (7)	0.911 (4)	0.0159 (19)
$Cr_{1.9}V_{0.1}S_3$ (V01)	5.93538 (7)	16.6887 (3)	509.156 (15)	12.95 (3)	0.846 (4)	0.042 (2)
$Cr_{1.95}V_{0.05}S_3$ (V005)	5.93574 (6)	16.6756 (3)	508.817 (14)	12.17 (3)	0.867 (4)	0.047 (3)
$Cr_{1.9}Ti_{0.1}S_3$ (Ti01)	5.93482 (7)	16.6932 (3)	509.195 (16)	15.55 (4)	0.831 (4)	0.050 (2)

Degrees of preferential orientation were determined from diffraction data of the sample pellets. All samples exhibited preferential orientation. Continued in supporting information Table SII
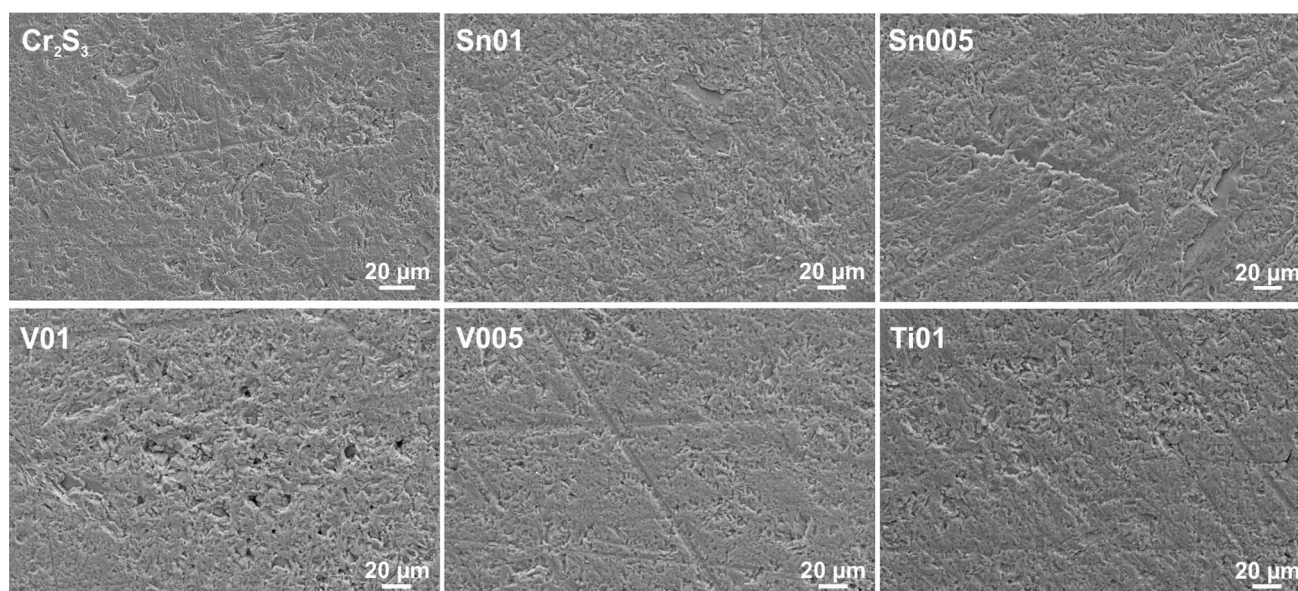
Fig. 3 Topographic SEM micrographs of pristine Cr_2S_3 in comparison with samples Sn01-Ti01. Except for the materials substituted with V and Ti, the surface topography is mostly comparable to pristine Cr_2S_3.

Transmission Electron Microscopy

A detailed study of the five samples was performed in order to investigate a possible influence of the substitutional elements on the crystal structure. As a result, it can be stated that none of the substitutional elements had a significant impact, as can be seen in the micrographs in Figure S6.[57] In comparison with simulated diffraction patterns of pristine Cr_2S_3 in the $R\bar{3}$ phase,[25,52] no significant deviations could be detected, indicating that the material kept its original phase in all five cases. However, certain zone axes, including $[\bar{1}11]$ and $[\bar{1}1\bar{1}]$, showed the appearance of superstructure reflections that vanished after short electron beam irradiation (see Fig. 4). The beam sensitivity and related phase transitions of comparable materials have been observed in previous studies,[58,59] for Cr_2S_3; however, it has not been studied in detail thus far.

High-resolution TEM (HRTEM) investigations revealed that the electron beam-induced phase transition occurred from the pristine $R\bar{3}$ to the non-equilibrium $P\bar{3}1c$ phase, which is a possible polymorph of Cr_2S_3 that is often found in material processed via FAST.[27] As apparent in the HRTEM micrograph in Fig. 4, left, the transition proceeded gradually and could be imaged with both phases coexisting side-by-side. The resulting FFT of the pristine (I) and transformed (II) material shows that the $R\bar{3}$ phase exhibited superstructure reflections with a tripling of the lattice parameter in the $[1\bar{1}1]^*$, $[0\bar{1}1]^*$ and $[10\bar{2}]^*$ directions. Electron beam irradiation caused these reflections to vanish during the transformation to $P\bar{3}1c$. Beam-induced phase transformations have been observed for similar materials[58–60] that share the same

basic structure as Cr_2S_3 with partially occupied layers containing mobile metal cations in between. If the material is irradiated, these cations may start to move and can order and rearrange into a different phase.

The transformation phenomenon could be directly observed in $Cr_{1.9}Sn_{0.1}S_3$ and $Cr_{1.95}V_{0.05}S_3$. Judging from the fact that it occurred for materials substituted with both compatible and incompatible substituents and following the results of previous studies,[30] it appears safe to assume that the reported transformation is a property of the pristine material Cr_2S_3 and not a result of the substitution of cations.

Accompanying the phase transformation, the occurrence of diffuse scattering on the positions of formerly present superstructure reflections could be observed, specifically in case of $Cr_{1.9}Sn_{0.1}S_3$. Closely observing Fig. 5, it can be seen that faint diffuse scattering was already visible in the initial $R\bar{3}$ phase after short beam irradiation, seemingly interconnecting the superstructure reflections. Following the phase transformation and the subsequent vanishing of superstructure reflections, the diffuse scattering gained in intensity and formed zig-zag shapes around the main structure reflections with local intensity maxima at former superstructure reflection positions.

The fact that diffuse scattering appears is linked to disorder of the structure, i.e. how metal cations are able to distribute within the system. If the material is irradiated, cations in the partially occupied layers gain mobility and are able to disorder which ultimately leads to the phase transformation. It is, however, possible that mobile cations and/or vacancies may order on a short-range scale and subsequently form dimers of either disordered cations or vacancies due
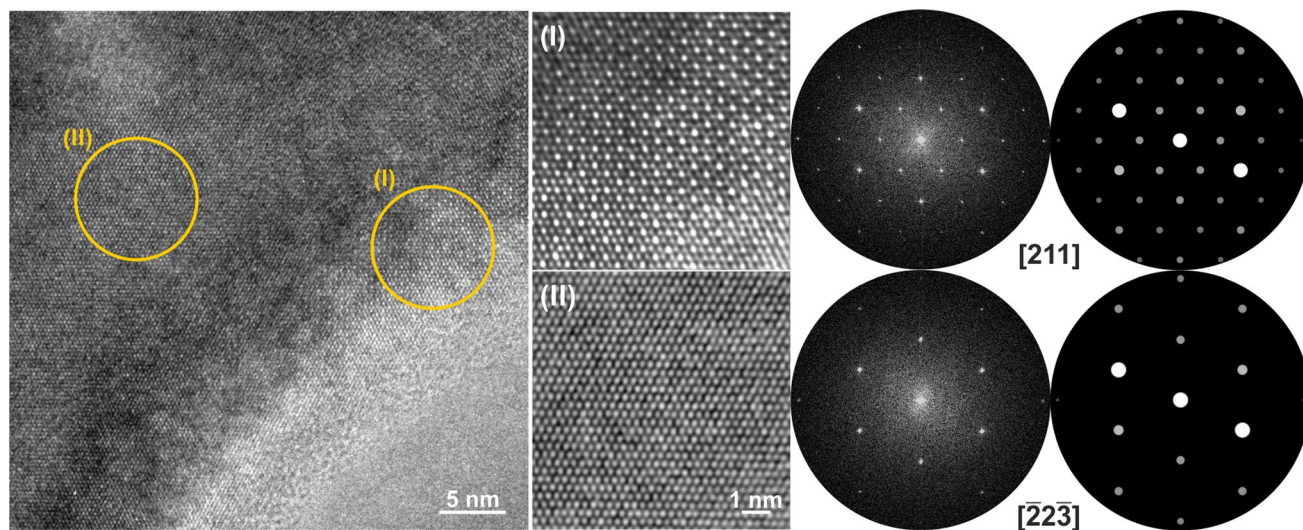
Fig. 4 HRTEM micrograph of $Cr_{1.9}Sn_{0.1}S_3$ during the phase transformation from (I) the $R\bar{3}$ phase to (II) $P\bar{3}1c$. Both coexisting phases are marked in the HRTEM micrograph and subsequently shown in magnified sections. On the right, their respective peak positions in FFT patterns are compared with reflection positions of simulated diffraction patterns of $R\bar{3}$ in [211] and $P\bar{3}1c$ in $[\bar{2}2\bar{3}]$, showing good agreement. Simulations were created using software described in Ref. 52, based on reference data from Ref. 25.
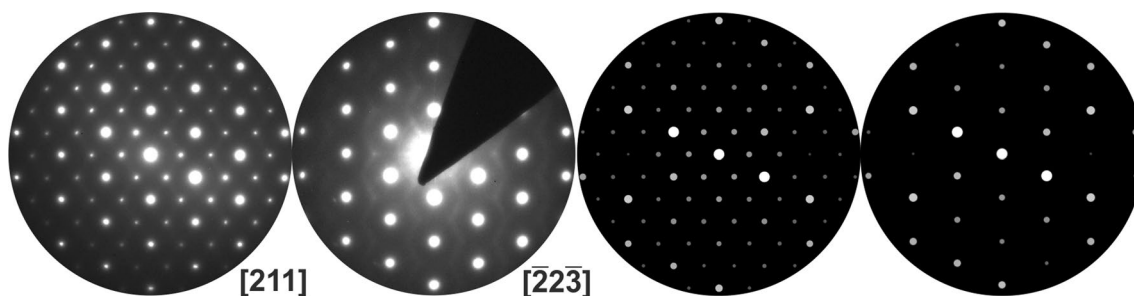
**Fig. 5** Occurrence of prominent diffuse scattering in $Cr_{1.9}Sn_{0.1}S_3$ (left) in comparison with simulated diffraction patterns (right). The material undergoes a phase transformation from the $R\bar{3}$ phase in [211] to $P\bar{3}1c$ in [$\bar{2}2\bar{3}$] where formerly present superstructure reflections vanish and give rise to diffuse scattering patterns with intensity maxima at their respective positions. The vertical, zig-zag-shaped pattern is already faintly visible in the top micrograph, but becomes increasingly intense after prolonged irradiation. Simulations were created using software described in Ref. 52, based on reference data from Ref. 25. Please note that for display purposes, the contrast of the micrographs has been non-linearly adjusted and does not represent actual experimental data.

Fig. 6 STEM-HAADF micrographs of $Cr_{1.9}Sn_{0.1}S_3$ (a) and $Cr_{1.95}Sn_{0.05}S_3$ (b). Both materials exhibited precipitations of Cr, which appear as grains of light Z-contrast embedded into the host material.
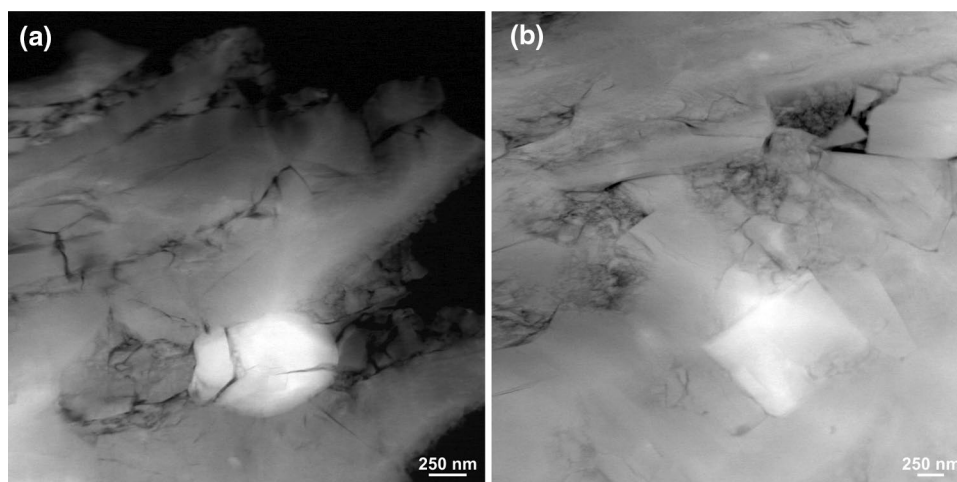
to energetically favorable conditions. These dimers cause a distortion in the local structure and may lead to the occurrence of diffuse scattering. Additionally, it is possible that the structure maintains order partially, which is expressed in the formation of microdomains that concentrate the intensity of the diffuse scattering on certain positions in reciprocal space.[61–63] The occurrence of diffuse scattering appears not to be restricted to the materials investigated in this study, as it has been observed in former studies of the pristine material as well as in a ternary Ni-Cr-S system that shares a similar sequence of layers.[59]

A deeper investigation via scanning TEM high-angle annular dark field imaging (STEM-HAADF) revealed that both Sn005 and Sn01 contained a loose distribution of precipitations with high atomic weight, as is shown in the STEM micrographs in Fig. 6. Originally believed to be precipitations of Sn, these appeared to be constituted of nearly elementary Cr. Large-scale SEM-EDX measurements (cf. Table II) further revealed that Sn005 and Sn01 contained almost no Sn, which could be confirmed by a subsequent

Table II Stoichiometry of the samples determined via SEM-EDX and XPS.

Compound	Stoichiometry determined via	
	SEM-EDX	XPS
$Cr_{1.9}Sn_{0.1}S_3$	$Cr_{2.07}Sn_{0.005}S_3$	$Cr_{1.80}Sn_{0.02}S_3$
$Cr_{1.95}Sn_{0.05}S_3$	$Cr_{2.03}Sn_{0.002}S_3$	$Cr_{1.89}Sn_{0.01}S_3$
$Cr_{1.9}V_{0.1}S_3$	$Cr_{1.98}V_{0.119}S_3$	–
$Cr_{1.95}V_{0.05}S_3$	$Cr_{2.07}V_{0.047}S_3$	–
$Cr_{1.9}Ti_{0.1}S_3$	$Cr_{2.04}Ti_{0.063}S_3$	–

The compositions of both V substitutions match the targeted stoichiometry closely, while Ti01 exhibits a deficiency in Ti. Both Sn substitutions appear with a surplus in Cr and barely-detectable traces of Sn. Note that deviations between the methods may arise because XPS is a highly surface-sensitive method with a significantly smaller interaction volume in contrast to EDX.

investigation of the same sample pellets via XPS. As the educts have been weighed stoichiometrically as in all other samples, where no precipitations could be found, an initial

surplus of Cr seems unlikely. Taking into account that both Sn005 and Sn01 lacked their respective content of Sn, it appears likely that Sn has reacted with the S atmosphere during synthesis and formed a tin sulfide,[64] which led to a subsequent surplus of Cr in the product. This surplus or respective deficiency of S has apparently been compensated in form of Cr-rich precipitations to restore bulk stoichiometry. Note that no traces of S-deficient Cr-S phases, e.g. Cr_3S_4 or Cr_5S_6,[65,66] could be found by XRD.

Thermoelectric Properties

The results of the thermoelectric measurements up to a temperature of 525 K are shown in Fig. 7. At room temperature, the thermoelectric properties of the Sn-substituted samples are improved the most. The electrical conductivity drastically increased up to 21 S cm^{-1} and decreased marginally with temperature. For comparison, pure Cr_2S_3 has an electrical conductivity of around 1 S cm^{-1}. The Seebeck coefficient decreased only slightly to around -320 µV K^{-1}, resulting in an increase of ZT to higher temperatures up to a maximum value of around 0.06. While the electrical properties of the Sn-containing material indicate metal-like behavior, the samples with Ti and V show semiconducting behavior. The substitution with the compatible cation V^{3+} led to a decrease
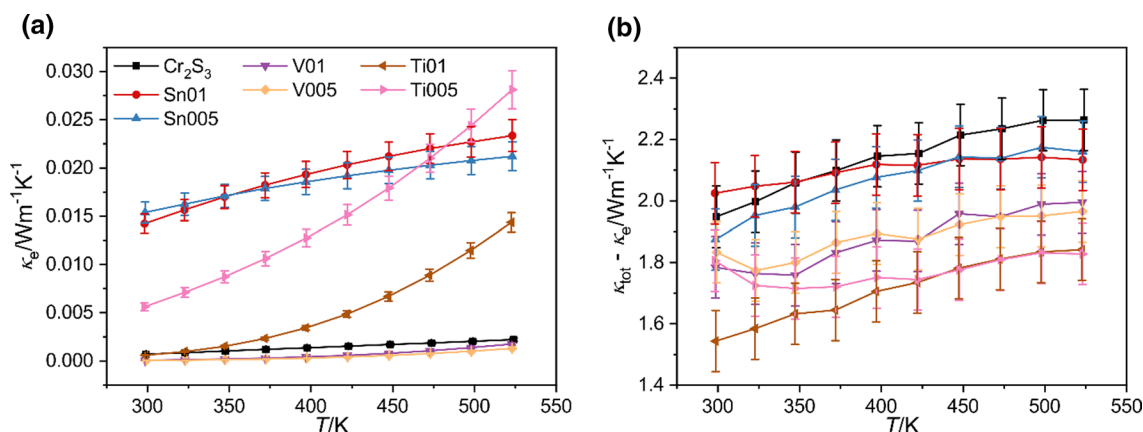
of the electrical conductivity to 0.11 S cm^{-1} and 0.07 S cm^{-1} for V01 and V005, respectively. With Ti, the thermoelectric properties could be improved. At higher temperatures, the electrical conductivity increases significantly and reaches a value of 22 S cm^{-1} at 525 K for Ti005. Both the Ti005 and the Sn substitutions reaches a maximum ZT value of 0.06 at 525 K. Compared to the pure Cr_2S_3 with a $ZT < 0.01$, the value could be increased drastically, but is still very low compared to established materials.

The thermal conductivity is at a low level for all samples with a maximum value of 2 W m^{-1} K^{-1} at RT. In comparison to pristine Cr_2S_3, it could be lowered with almost all substitutions, with the exception of Sn01 at room temperature. The lowest value could be achieved for Ti01, which reached a thermal conductivity below 1.6 W m^{-1} K^{-1} at RT. Although the electrical conductivity increases only for the Ti-substituted samples, the thermal conductivity increases with temperature in all samples (Fig. 7c). For a more detailed analysis, the electronic thermal conductivity was estimated according the Wiedemann–Franz law $\kappa_e = L\sigma T$. For a first approximation, the constant Lorenz number for metals of $L = 2.44 \times 10^{-8}$ V^2 K^{-2} was assumed. By subtracting the electronic thermal conductivity from the total thermal conductivity, the lattice thermal conductivity and the bipolar thermal conductivity are obtained ($\kappa_{tot} - \kappa_e$
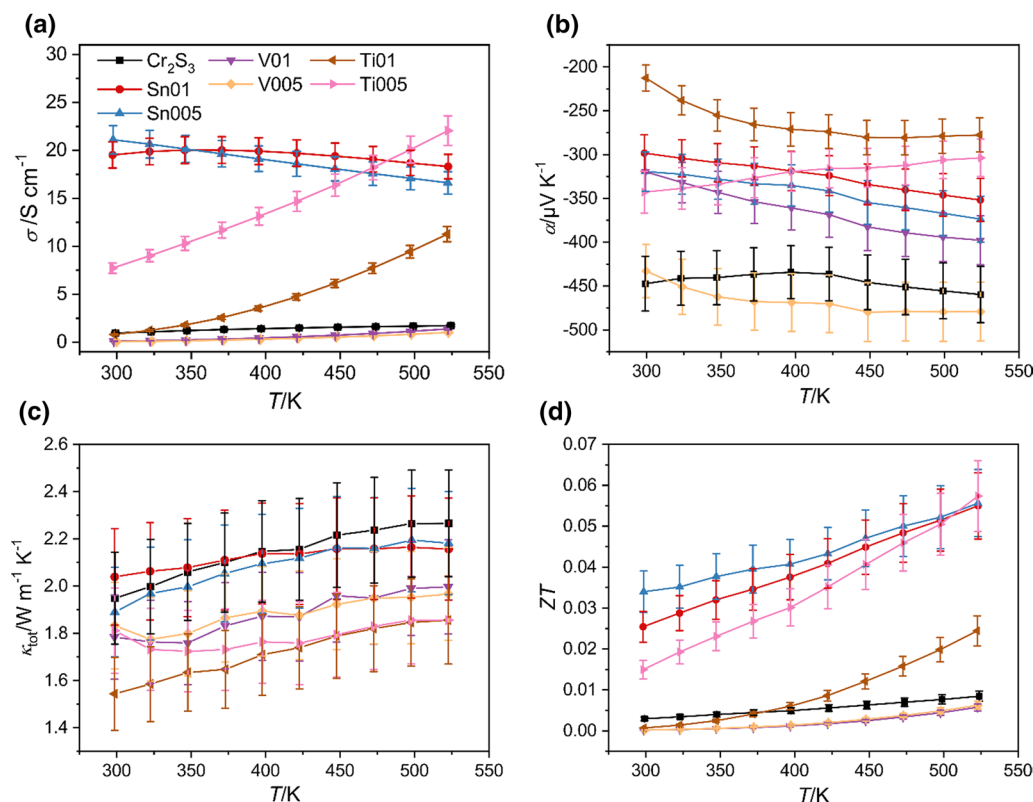
Fig. 7 Electrical conductivity σ (a), Seebeck coefficient α (b), thermal conductivity κ (c) and ZT values (d) for pure Cr_2S_3 and the substitutions.

(a)

(b)

Fig. 8 Detailed view of the thermal conductivity's behavior with temperature, divided into electrical contribution κ_e (a) as well as lattice contribution with bipolar conductivity $\kappa_{tot} - \kappa_e$ (b).

$= \kappa_l - \kappa_{bi}$). However, at low temperatures, the bipolar conductivity is negligible. Thus, Fig. 8 shows that although κ_e increases with temperature, the lattice thermal conductivity is the main contributor to the total thermal conductivity κ_{tot}. The low and temperature-independent thermal conductivity is comparable to the properties of complex materials such as glass and indicates multiple scattering processes. This unusual trend is often observed for chromium sulfides and selenides, but could not be clarified in detail.[26,67,68]

Conclusions

It could be demonstrated that cation substitution in $R\bar{3}$-Cr_2S_3 with elements of different structural compatibilities influences the material's properties to different, albeit marginal, degrees. Substitution with compatible V^{3+} and semi-compatible Ti^{4+} cations led to a slight increase in unit cell volume as well as a partial formation of disorder or $P\bar{3}1c$ phase after sintering. While the electric properties generally deteriorated with V substitution despite its compatibility, a slight improvement in electrical conductivity could be achieved via substitution with Ti, especially in low concentration. In case of the incompatible Sn^{4+}, it appeared that the Sn content had reacted to a byproduct during synthesis, as no traces could be detected in the resulting samples. The lack of Sn, however, did lead to interesting properties, as the highest improvement in thermoelectric properties could be achieved in this area with a doubled or almost tripled electrical conductivity in the case of low concentration. This effect may be linked to a high preferred orientation of the samples as well as Cr precipitations which could be found during TEM investigations. Interestingly, the highest effects

on the thermoelectric properties were always achieved with the lower concentration of 2.5% of the respective substituting element. All samples further appeared to exhibit a phase transformation during electron beam irradiation, caused by the movement of cations in partially occupied layers. In addition, the occurrence of diffuse scattering could be observed, indicating a non-random repositioning of cations with a degree of short-range ordering and formation of microdomains.

References

1. Z.-H. Ge, L.-D. Zhao, D. Wu, X. Liu, B.-P. Zhang, J.-F. Li and J. He, Low-cost, abundant binary sulfides as promising thermoelectric materials. *Mater. Today* 19, 4 (2016).

2. D.M. Rowe, *CRC Handbook of Thermoelectrics* (Boca Raton: CRC Press, 1995).

3. J.D. Koenig, M. Winkler, S. Buller, W. Bensch, U. Schuermann, L. Kienle and H. Boettner, Bi$_2$Te$_3$-Sb$_2$Te$_3$ Superlattices grown by nanoalloying. *J. Electron. Mater.* 40, 1266 (2011).

4. U. Schuermann, M. Winkler, J.D. Koenig, X. Liu, V. Duppel, W. Bensch, H. Boettner and L. Kienle, In situ TEM investigations on thermoelectric Bi$_2$Te$_3$/Sb$_2$Te$_3$ multilayers. *Adv. Eng. Mater.* 14, 139 (2012).

5. A.-L. Hansen, T. Dankwort, M. Winkler, J. Ditto, D.C. Johnson, J.D. Koenig, K. Bartholomé, L. Kienle and W. Bensch, Synthesis and thermal instability of High-Quality Bi$_2$Te$_3$/Sb$_2$Te$_3$ superlattice thin film thermoelectrics. *Chem. Mater.* 26, 6518 (2014).

6. C. Chiritescu, D.G. Cahill, N. Nguyen, D. Johnson, A. Bodapati, P. Keblinski and P. Zschack, Ultralow thermal conductivity in disordered, layered WSe$_2$ crystals. *Science* 315, 351 (2007).

7. G.J. Snyder and E.S. Toberer, Complex thermoelectric materials. *Nat. Mater.* 7, 105–114 (2008).

8. P. Vaqueiro, A.V. Powell, A.I. Coldea, C.A. Steer, I.M. Marshall, S.J. Blundell, J. Singleton and T. Ohtani, Colossal magnetoresistance in the layered chromium sulfide Cr$_2$S$_{3-x}$ (x = 0.08). *Phys. Rev. B* 64, 132402 (2001).

9. C.F. van Bruggen, M.B. Vellinga and C.J. Haas, Semiconducting and magnetic properties of rhombohedral Cr$_2$S$_3$. *J. Solid State Chem.* 2, 303 (1970).

10. T.E. Engin, A.V. Powell and S. Hull, Structural, magnetic, and electronic properties of V$_x$Cr$_{2-x}$S$_3$ (0 < x < 2). *Chem. Mater.* 20, 2039 (2008).

11. A.V. Powell, P. Vaqueiro and A. McDowall, Structure–property relationships in ordered-defect sulphides. *Solid State Ion.* 172, 469 (2004).

12. C. Lovasz and H.D. Lutz, Zur Struktur der Chromsulfide und des NiCr$_2$S$_4$. *Z. Naturforsch.* 25b, 313 (1970).

13. H. Haraldsen and A. Neuber, Magnetochemische Untersuchungen. XXVI. Eine magnetische Untersuchung des Systems Chrom-Schwefel. *Z. Anorg. Allg. Chem.* 234, 337 (1937).

14. T.J.A. Popma and C.F. van Bruggen, Structural and magnetic phase transitions of chromium sulfides Cr$_{1-x}$S with 0 ⩽ x ⩽ 0·12. *J. Inorg. Nucl. Chem.* 31, 73 (1969).

15. T.J.A. Popma, C. Haas and B. van Laar, Spin structure and magnetic anisotropy of Cr$_5$S$_6$ and rhombohedral Cr$_2$S$_3$. *J. Phys. Chem. Solids* 32, 581 (1971).

16. B.L. Morris, R.H. Plovnick and A. Wold, Magnetic susceptibility of some transition metal chalcogenides having the Cr$_3$S$_4$ structure. *Solid State Commun.* 7, 291 (1969).

17. W. Bensch, H. Luehmann, C. Naether and H. Huppertz, The crystal structure of non-stoichiometric monoclinic Cr$_{5+x}$S$_8$ (x = 020 and 026) prepared under high pressure and high temperature. *Z. Kristallogr.* 217, 510 (2002).

18. A.W. Sleight and T.A. Bither, New chromium chalcogenides prepared at high pressure and the crystal growth of chromium sesquisulfide. *Inorg Chem.* 8, 566 (1969).

19. K.R. Pisharody, Thermoelectric properties of chromium sulfoselenides. *J. Solid State Chem.* 30, 149 (1979).

20. J.R. Sootsman, D.Y. Chung and M.G. Kanatzidis, Alte und neue Konzepte für thermoelektrische Materialien. *Angew. Chem.* 121, 8768 (2009).

21. A. Maignan, E. Guilmeau, F. Gascoin, Y. Bréard and V. Hardy, *Sci. Technol. Adv. Mater.* 13, 53003 (2012).

22. N. Tsujii, H. Kitazawa and G. Kido, Insulator to metal transition induced by substitution in the nearly two-dimensional compound CuCr$_{1-x}$V$_x$S$_2$. *Phys. Status Solidi* 3, 2775 (2006).

23. S.L. Holt, R.J. Bouchard and A. Wold, Ternary chalcogenides of vanadium and chromium. *Solid State Commun.* 4, 4 (1966).

24. A.V. Powell, P. Vaqueiro and T. Ohtani, Thermopower across the insulator-metal divide in NiCr$_{2-x}$V$_x$S$_4$ (0 ⩽ x ⩽ 2). *Phys. Rev. B* 71, 125120 (2005).

25. F. Jellinek, The structures of the chromium sulphides. *Acta Cryst.* 10, 620 (1957).

26. A. Maignan, E. Guilmeau, F. Gascoin, Y. Bréard and V. Hardy, Revisiting some chalcogenides for thermoelectricity. *Sci. Technol. Adv. Mater.* 13, 53003 (2012).

27. A. Maignan, Y. Bréard, E. Guilmeau and F. Gascoin, Transport, thermoelectric, and magnetic properties of a dense Cr$_2$S$_3$ ceramic. *J. Appl. Phys.* 112, 13716 (2012).

28. D. Babot, G. Peix and M. Chevreton, Transition métal-semiconducteur das les composés Cr$_2$S$_{3-x}$Se$_x$ et Cr$_{2+e}$Se$_3$. *J. Phys. Colloq.* 37, C4-111 (1976).

29. D. Babot and M. Chevreton, Conductibilité electrique aux basses températures des composés binaires Cr$_2$X$_3$ et Cr$_3$X$_4$ (X = S, Se ou Te). *J. Solid State Chem.* 8, 166 (1973).

30. D. Groeneveld, H. Groß, A.-L. Hansen, T. Dankwort, J. Hansen, J. Woellenstein, W. Bensch, L. Kienle, J. D. Koenig, High-pressure sintering of rhombohedral Cr$_2$S$_3$ using titanium–zirconium–molybdenum tools. *Adv. Eng. Mater.* 21, 1900430 (2019).

31. N.A. Heinz, T. Ikeda, Y. Pei and G.J. Snyder, Applying quantitative microstructure control in advanced functional composites. *Adv. Funct. Mat.* 24, 2135 (2014).

32. J. Androulakis, C.-H. Lin, H.-J. Kong, C. Uher, C.-I. Wu, T. Hogan, B.A. Cook, T. Caillat, K.M. Paraskevopoulos and M.G. Kanatzidis, Spinodal decomposition and nucleation and growth as a means to bulk nanostructured thermoelectrics: enhanced performance in Pb$_{(1-x)}$Sn$_{(x)}$Te-PbS. *J. Am. Chem. Soc.* 129, 9780 (2007).

33. Z.A. Munir and U. Anselmi-Tamburini, The effect of electric field and pressure on the synthesis and consolidation of materials: a review of the spark plasma sintering method. *J. Mater. Sci.* 41, 763 (2006).

34. A. Shakouri, Recent developments in semiconductor thermoelectric physics and materials. *Annu. Rev. Mater. Res.* 41, 399 (2011).

35. M. Taniguchi, M. Wakihara and Y. Shirai, Growth of single crystals of vanadium sulfides and their electrical conductivity. *Z. Anorg. Allg. Chem.* 461, 234 (1980).

36. W. Bensch and R. Schloegl, An X-ray and ultraviolet photoemission study of vanadium sulfides in the series VS$_{1.0}$-VS$_{1.60}$. *J. Solid State Chem.* 107, 43 (1993).

37. N.F. Mott, Conduction in glasses containing transition metal ions. *J. Non Cryst. Solids* 1, 1 (1968).

38. F. Jellinek, Sulfides of transition metals of groups 4, 5 and 6. *Arkiv Kemi* 20, 447 (1963).

39. A.D. Wadsley, Partial order in the non-stoichiometric phase Ti$_{2+x}$S$_4$(0.2 < x < 1). *Acta Cryst.* 10, 715 (1957).

40. M. Onoda, M. Saeki and I. Kawada, Superstructures of Ti$_2$S$_3$ (4H). *Z. Anorg. Allg. Chem.* 457, 62 (1979).

41. H.G. von Schnering and H. Wiedemeier, The high temperature structure of ß-SnS and ß-SnSe and the B16-to-B33 type λ-transition path. *Z. Kristallogr.* 156, 143 (1981).

42. B.F. Bilenkii, A.G. Mikolaichuk and D.M. Freik, Struktur und optische Eigenschaften von epitaxialen SnTe- SnSe- und SnS-Schichten. *Phys. Status Solidi* 28, K5 (1968).

43. R.E. Abutbul, A.R. Garcia-Angelmo, Z. Burshtein, M.T.S. Nair, P.K. Nair and Y. Golan, Crystal structure of a large cubic tin monosulfide polymorph: an unraveled puzzle. *CrystEngComm* 18, 5188 (2016).

44. D. Mootz and R. Kunzmann, Die Kristallstruktur von Sn_2S_3, einer dritten Phase im System Zinn-Schwefel. *Acta Cryst.* 15, 913 (1962).

45. Alan Coelho, *Topas Academic v6* (Coelho Software, 2016).

46. jEdit, http://www.jedit.org/index.php?page=features, Accessed 21 Nov 2018.

47. H. Sawada, Electron density studies of spinels: zinc chromium oxide. *Mater. Res. Bull.* 32, 873 (1997).

48. A. March, Mathematische Theorie der Regelung nach der Korngestalt bei affiner Deformation. *Z. Krist.* 81, 285 (1932).

49. W.A. Dollase, Correction of intensities for preferred orientation in powder diffractometry: application of the March model. *J. Appl. Cryst.* 19, 267 (1986).

50. E. Zolotoyabko, Determination of the degree of preferred orientation within the March-Dollase approach. *J. Appl. Cryst.* 42, 513 (2009).

51. D.R.G. Mitchell and B. Schaffer, Scripting-customised microscopy tools for Digital Micrograph™. *Ultramicroscopy* 103, 319 (2005).

52. P.A. Stadelmann, EMS—a software package for electron diffraction analysis and HREM image simulation in materials science. *Ultramicroscopy* 21, 131 (1987).

53. G. Bergerhoff, M. Berndt and K. Brandenburg, Evaluation of crystallographic data with the program DIAMOND. *J. Res. Natl. Inst. Stand. Technol.* 101, 221 (1996).

54. L.J. van der Pauw, A method of measuring specific resistivity and Hall effect of discs of arbitrary shape. *Philips Res. Rep.* 13, 1 (1958).

55. O. Guillon, J. Gonzalez-Julian, B. Dargatz, T. Kessel, G. Schierning, J. Räthel and M. Herrmann, Field-assisted sintering technology/spark plasma sintering: mechanisms, materials, and technology developments. *Adv. Eng. Mater.* 16, 7 (2014).

56. D. Dudina and B. Bokhonov, Elimination of oxide films during Spark Plasma Sintering of metallic powders: a case study using partially oxidized nickel. *Adv. Powd. Technol.* 28, 641 (2017).

57. H. Groß, *Strukturelle Charakterisierung Chromchalkogenidbasierter Thermoelektrika mittels Transmissionselektronenmikroskopie*. Kiel University (2021).

58. A.-L. Hansen, T. Dankwort, H. Groß, M. Etter, J.D. Koenig, V. Duppel, L. Kienle and W. Bensch, Structural properties of the thermoelectric material $CuCrS_2$ and of deintercalated Cu_xCrS_2 on different length scales: X-ray diffraction, pair distribution function and transmission electron microscopy studies. *J. Mater. Chem. C* 5, 9331 (2017).

59. H. Groß, T. Dankwort, A.-L. Hansen, U. Schuermann, V. Duppel, M. Poschmann, A. Meingast, D. Groeneveld, J.D. Koenig, W. Bensch and L. Kienle, Purification by SPS and formation of a unique 3D nanoscale network: the showcase of Ni-Cr-S. *J. Mater. Chem.* C7, 15188 (2019).

60. P. Vaqueiro, A.V. Powell and B. Lebech, Order-disorder transitions in $NiCr_2S_4$. *Physica B* 276–278, 238 (2000).

61. S. Vensky, L. Kienle, R.E. Dinnebier, A.S. Masadeh, S.J.L. Billinge and M. Jansen, The real structure of Na_3BiO_4 by electron microscopy, HR-XRD and PDF analysis. *Z. Kristallogr.* 220, 231 (2005).

62. M.A. Castellanos Román, A.M. de León Guevara, J. Guzmán-Mendoza, L. Banos, J.L. Heiras-Aguirre and A. Huanosta-Tera, Diffuse electron scattering of a region in the system Li_2SnO_3-CoO. *Acta Mater.* 51, 2125 (2003).

63. R. de Ridder, G. van Tendeloo and S. Amelinckx, A cluster model for the transition from the short-range order to the long-range order state in f.c.c. based binary systems and its study by means of electron diffraction. *Acta Cryst.* A32, 216 (1976).

64. L.A. Burton and A. Walsh, Phase stability of the earth-abundant tin sulfides SnS, SnS_2, and Sn_2S_3. *J. Phys. Chem. C* 116, 24262 (2012).

65. A. El Goresy, G. Kullerud, Phase relations in the system Cr-Fe-S, in *Meteorite Research* (1969), p. 638.

66. P. Waldner and W. Sitte, Sulfur solubility of liquid and solid Fe-Cr alloys: a thermodynamic analysis. *Int. J. Mater. Res.* 106, 352 (2015).

67. G.J. Snyder, T. Caillat and J.-P. Fleurial, Thermoelectric properties of Cr_3S_4-type selenides. *MRS Proc.* 545, 333 (1998).

68. S. Bhattacharya, R. Basu, R. Bhatt, S. Pitale, A. Singh, D.K. Aswal, S.K. Gupta, M. Navaneethan and Y. Hayakawa, $CuCrSe_2$: a high performance phonon glass and electron crystal thermoelectric material. *J. Mater. Chem. A* 1, 11289 (2013).